Infrared fingerprints of water collective dynamics indicate proton transport in biological systems

Z. V. Gagkayeva ◉, B. P. Gorshunov, A. Ye. Kachesov, and K. A. Motovilov ◉[*]

Center for Photonics and 2D Materials, Moscow Institute of Physics and Technology (National Research University), 9 Institutskiy per., Dolgoprudny, Moscow Region 141701, Russian Federation

Recent publications on spectroscopy of water layers in water bridge structures revealed a significant enhancement of the proton mobility and the dielectric contribution of translational vibrations of water molecules in the interfacial layers compared to bulk water. Herewith, the results of long-term studies of proton dynamics in solid-state acids have shown that proton mobility increases significantly with the predominance of hydronium, but not Zundel, cations in the aqueous phase. In the present work, in the light of these data, we reanalyzed our previously published results on broadband dielectric spectroscopy of bovine heart cytochrome c, bovine serum albumin, and the extracellular matrix and filaments of *Shewanella oneidensis* MR-1. We revealed that, just as in water bridges, an increase in electrical conductivity in these systems correlates with an increase in the dielectric contribution of water molecular translational vibrations. In addition, the appearance of spectral signatures of the hydronium cations was observed only in those cases when the system revealed noticeable electrical conductivity due to delocalized charge carriers.

I. INTRODUCTION

In recent years, electrically conductive objects of bioorganic origin have become a hot topic within a number of industrial and research sectors [1,2]. In the rapidly evolving field of bioelectronics, the question of charge transport mechanisms in bio-organic materials still plays a crucial role. This is motivated by the need for appropriate interfacial materials which would allow connecting electrical circuits with biological systems on the one hand [3–11] and a fundamental interest on the other [12–15]. With skyrocketing levels of electronic waste production [16], biodegradable alternatives to traditional materials used in mass consumer electronics, also known as green electronics [17], became necessary to reduce electronic waste. This issue has also stimulated a search for the relevant materials among various compounds of bio-organic origin [15,18–25].

Regardless of the charge-carrier type or transport mechanism in a particular bio-organic material, water is involved directly or indirectly in the electrical conductivity process [26–29]. In soft matter, water contacts polar groups of biomolecules and may exist in various bound states, forming protein hydration shells, polygonal structures on the molecular surface, large clusters, and hydration networks extended through the bulk of the material [30–33]. If the medium contains an excess of protons, water molecules may combine and form a variety of aqueous proton cations $H^+\text{-}(H_2O)_n$ such as hydronium (H_3O^+), Zundel ($H_5O_2^+$), Eigen ($H_9O_4^+$) ions, etc. [34]. Currently, the $H_5O_2^+$ species is regarded as the simplest stable ion of the above series in aqueous media [35–37]. However, its predominance in solid-state acids is associated with a decrease in proton mobility, where H_3O^+ species becomes the preferable ion to perform more effective proton transportation [38–44].

Among bio-organic systems of particular interest are electrogenic bacteria, such as *Geobacter sulfurreducens* or *Shewanella oneidensis*, whose extracellular outgrowths are capable of electron transfer [12,28,45,46]. Our previous broadband dielectric spectroscopy studies [47,48] showed that *S. oneidensis* MR-1 extracellular matrix and filaments (EMF) at temperatures above 250 K demonstrate spectral features typical for Drude-type electrical conductivity. We note that spectroscopy provides an effective tool to reliably detect the presence of delocalized charge carriers in the material as evidenced by the measured AC conductivity that is not changing its value over decades of frequency and matching the DC conductivity (zero-frequency limit), following the conductivity model developed by Drude; see Ref. [49]. Interestingly, the appearance of Drude-like conductivity always correlated with the rise of the terahertz shoulder of Debye relaxation of bound water [50] and the presence of translational and librational modes of water molecules in the infrared region. The substantive discussions about transport mechanisms in EMF lack a clear understanding of its structure and composition. We can only expect that multiheme cytochromes (OmcA and Mtr-family) are the main protein components of EMF since their signatures were clearly observed in the Raman spectra [28], and they are the main components of conductive cellular outgrowth of *S. oneidensis* [51]. To compare EMF data with well-characterized reference materials, we also added to the study bovine heart cytochrome c (CytC) and bovine serum albumin (BSA). The first material is a classical participant of electron transfer in the mitochondrial respiratory chain containing a heme prosthetic group like bacterial OmcA and Mtr-proteins. In its turn, BSA is a ubiquitous protein responsible for the blood osmolality and transportation of various substrates. BSA has no prosthetic groups and no relation

*k.a.motovilov@gmail.com

to charge-transfer processes. As expected, CytC showed behavior similar to that of EMF, but the registered electrical conductivity was orders of magnitude lower, and the subterahertz (below 100 GHz) Debye relaxation of water was somewhat weaker [48]. In BSA, on the contrary, neither a Drude-like response nor Debye relaxation could be observed [48]. Nevertheless, it has not been investigated how water affects conductivity in these materials or if the aqueous cations influence charge transport mechanisms. Continuing a series of studies on EMF, CytC, and BSA dielectric properties, this work focuses on the relationship between the spectroscopic signatures of aqueous protonic species in these materials and their charge transport characteristics. We utilize infrared spectroscopy, which is a well-proven tool for studying protein systems [52,53].

Unveiling the mechanism of charge transport and the nature of charge carriers is a fundamental problem in condensed-matter physics. It is not easy to cover the entire range of specific issues related to this field. However, the present work highlights to the interested reader at least the key points, and for a deeper acquaintance, one can refer to the more specialized literature. In general, the problems of determining the charge transport mechanism and the type of charge carriers are interrelated, regardless of whether a particular material is a bio-organic or a classical solid state. Ideally, the researcher should measure the material's conductivity values over as broad temperature and frequency ranges as possible [54,55]. In case the conductivity component is associated with ionic charge carriers, the data on electrical impedance spectroscopy (EIS), pulsed-field gradient nuclear magnetic relaxation (PFG NMR), quasielastic neutron scattering (QENS), and, of course, Hall effect measurements will also be essential and quite affordable. An experimenter working with a bio-organic system faces a series of additional problems, which are specific for such objects:

(1) Relatively low conductivity makes standard techniques like Hall effect measurements inapplicable for most types of biomaterials.

(2) Series of phase transitions can lead to qualitative change of the conductivity mechanism. The corresponding restriction of the temperature range between specific temperatures can make it impossible to identify the charge transport mechanism reliably. For example, one can encounter serious difficulties determining the dimensionality n of hopping conductivity, whose temperature dependence is given as $\sigma_{DC} \propto T^{\frac{1}{n+1}}$ [56].

(3) Bio-organic materials cannot be heated significantly above room temperature without irreversible decomposition.

(4) The presence of water can crucially affect various properties of bio-organic materials, including electrical conductivity. Therefore, performing good experiments requires precisely controlling the water content in a sample.

As a result, one usually is forced to deal with limited, sometimes too general information, like whether the material contains free carriers or not. Also, the typical spectroscopic signature of free-carrier response, the dispersionless real part σ' of AC conductivity [49], provides no information about the origin and type of charge carriers. EIS can determine the number of types of charge carriers, in some cases being, however, unable to identify their origin [57]. The use of EIS for studies of hydrated *S. oneidensis* single extracellular filament can be found in Ref. [28]. QENS [58], PFG NMR [59,60], μSR (muon spin relaxation) [29,61], and AC/DC measurements with contacts made of proton-conducting material like palladium hydride PdH$_x$ [62,63] provide essential information about proton-based diffusion–relaxation–mobility–conductivity in the material. Using these techniques, in a reasonably large number of cases, especially when protons and electrons are the main charge carriers, one can estimate the ratio of corresponding contributions. It should be noted that applying a four-contact scheme to determine the material's conductivity (Van der Pauw approach) is mandatory when one deals with macroscopic flat samples, like pressed pellets studied by us [48]. An example of the natural pigment melanin shows that the results of two- and four-contact measurements can be fundamentally different and lead to entirely divergent conclusions [64]. When the sample has nanoscale dimensions (single bio-organic molecule or bacterial nanofilament), the Van der Pauw scheme application becomes impossible. In this case, one has to deal with many related problems. The top methods in this area came from molecular electronics and are well described in a recent review [65]. They include chemical modification of the material aimed at making covalent bonding with a conductive probe of the tunnel or atomic force microscope. However, if there is a solid need to exclude chemical modification of nanosize samples, some novel approaches from green lithography may help. The recently developed chitosan-based technique [66] made it available to perform conductivity measurements of metastable supramolecular bio-organic objects like individual brain microtubules without apparent chemical modifications.

II. EXPERIMENT SECTION

A. Samples

The *S. oneidensis* MR-1 strain was obtained in Research Institute for Genetics and Selection of Industrial Microorganisms and then its extracellular matrix and filaments were isolated as described in previous work [47,48]. Bovine serum albumin was purchased from Amresco (code 0332), and CytC was purchased from Sigma-Aldrich (code C3131). The EMF, CytC, and BSA samples were lyophilized powders pressed into pellets or prepared as thin films on polyethylene with a diameter of 1 cm and a thickness of 100–150 μm for films and 1 mm for pellets. For hydration control, all the samples were kept inside sealed jars above saturated salt solutions until reaching a weight that did not change with time. Thermogravimetry and element analysis were used to characterize the samples.

B. Experiment equipment

Fourier-transform infrared spectrometer Vertex 80V, Bruker, was used to study infrared vibrational modes of EMF, CytC, and BSA samples in the frequency range from 100 to 8000 cm^{-1}. For the low-temperature measurements down to 5 K, a helium flow cryostat was used. To obtain information about highly absorbing regions of the spectra, the transmission coefficient data were supplemented by the measurements in reflection mode. Reflection data were also helpful while fitting
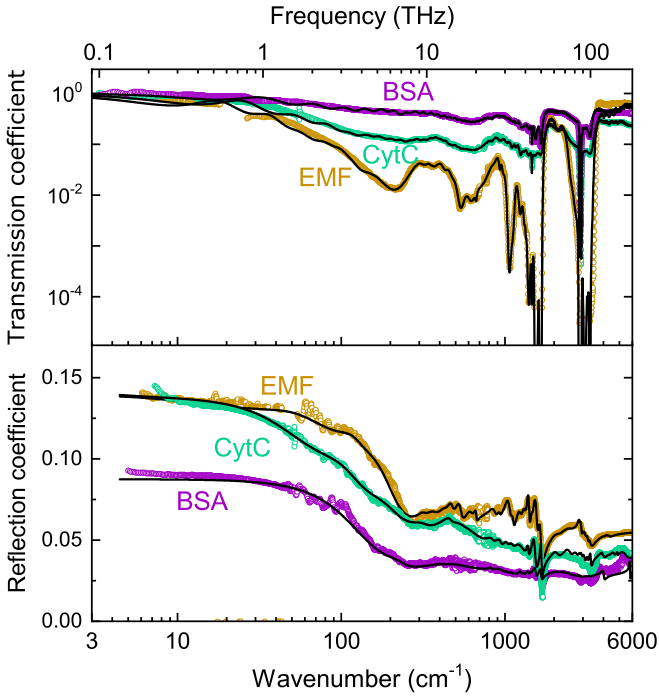
FIG. 1. Terahertz-infrared spectra of transmission and reflection coefficients of EMF, CytC, and BSA samples measured at 300 K. Solid black lines show least-square fitting results as described in the text.

the spectral regions near polyethylene absorption bands. Both transmittance and reflectance spectra of all three samples were processed with a least-square method using the Lorentz model to describe every absorption line:

$$\varepsilon^*(\nu) = \varepsilon' + i\varepsilon'' = \frac{f}{(\nu_0^2 - \nu^2) + i\nu_0\gamma},$$

where ε^* is complex dielectric permittivity with its real ε' and imaginary ε'' parts, ν_0 is the frequency, $f = \Delta\varepsilon\nu_0^2$ is the oscillator strength, and γ is the damping factor. Such analysis of the spectra with numerous independent absorption resonances is a typical procedure in spectroscopic studies that allows extracting parameters of each resonance.

III. RESULTS

The infrared transmittance and reflectance spectra of EMF, CytC, and BSA measured at room temperature ($T = 300$ K) are shown in Fig. 1 with fitting results. In the frequency ranges where other research groups have previously published the data, our results on CytC and BSA coincide with the literature parameters. For instance, the spectrum of CytC shows characteristic bands of amide I at frequencies close to 1650 cm⁻¹ and amide II band and antisymmetric stretching vibrations line of COO⁻ group near 1550 cm⁻¹ [52,67–70]. Spectral features that correspond to amide I (1660 cm⁻¹), amide II (1540 cm⁻¹), N-H stretching (3320 cm⁻¹, 3063 cm⁻¹), and COO⁻ stretching (1398 cm⁻¹) vibrations [71] are revealed in the spectra of BSA.

We have already published the characteristics of EMF, CytC, and BSA absorption lines with resonance frequen-

cies located in the midinfrared spectral region (from 1000 to 6000 cm⁻¹) [47]. In that work, we focused on studying the relationship between spectral signatures of low-frequency conductivity and the terahertz (infrared) response of bound water molecules. The other midinfrared absorption bands have not been analyzed, and no far-infrared data were included in the publication. Still, while the analysis of every single infrared absorption line is beyond the scope of the present paper, some far- and midinfrared bands discussed below are of greater interest for the understanding of charge transport mechanism and bound water properties in bacterial filaments and proteins.

For example, these include the absorption peak near 530 cm⁻¹, associated with the hydronium response. Hydronium, or the oxonium ion H₃O⁺, which is formed as a result of water molecule protonation, has a few infrared features including ν_2 vibration-inversion mode, or the so-called umbrella mode, with two bands: 1⁺–0⁻ transition at frequencies 511–560 cm⁻¹ and 1⁻–0⁺ transition at frequencies 954–1075 cm⁻¹ [72]. The pronounced peak observed in the infrared spectra of EMF at 532 cm⁻¹ highly likely corresponds to the 1⁺–0⁻ band. One can also see the same peak (at a frequency 531 cm⁻¹), but of lower intensity in the spectrum of CytC. For BSA, there is an absorption line at 525 cm⁻¹ whose oscillator strength is orders of magnitude weaker (see Table I). As for the 1⁻–0⁺ band, there are peaks of similar intensity at 1067, 1029, and 1041 cm⁻¹ for EMF, CytC, and BSA, respectively, each again with significantly smaller strength. However, a reliable determination of these lines' precise origin is complicated by the proximity of other vibrations, such as ν_{as}(OHO) of Zundel ion [73,74] or protein NH₃⁺ rocking vibrations [52].

According to Stoyanov *et al.* [75], there is another characteristic group of absorption bands of hydronium ion, which includes δ_{as}(H₃O⁺) that is located at 1597–1710 cm⁻¹ and associated with H₃O⁺ bending, and $\nu_1(A_1) + \nu_3(E)$ that forms a broad and intense band at 2536–3010 cm⁻¹ and is referred to the O-H stretching vibrations. The latter might have manifested themselves in the transmissivity spectrum of EMF as a broad and intense band at 2776 cm⁻¹, and in CytC and BSA spectra, as weaker bands at 2742 cm⁻¹. Analysis of the origin of the peak at 1650–1660 cm⁻¹ is more difficult because of the pronounced absorption due to amide I vibration at ~1650 cm⁻¹, which is characteristic of most proteins [53]. At low temperatures, the described peaks freeze out, corresponding to the freezing of bound water in the samples (Fig. 2).

Another aqueous cation that can participate in proton transport processes in materials that are organic and inorganic proton conductors is the Zundel ion, H₅O₂⁺. However, the discernment of its infrared absorption lines is still a matter of debate, since it is complicated by numerous overlaps with proteins and the Zundel ion lines [76]. The Zundel ion is formed as a cluster of two water molecules with a proton distributed between them and forming short, strong, low-barrier (SSLB) H bonding with water O atoms [35,36,77–80]. The presence of Zundel ion in hydration networks within a condensed material shows up as a group of infrared bands associated with O–H⁺–O group vibrations: the most intense one at 1000–1160 cm⁻¹ corresponding to ν_{as}(OHO) mode; well-defined bands at 1672–1700 and 860–995 cm⁻¹; weak bands

TABLE I. The parameters of infrared absorption lines from the transmissivity spectra of EMF, CytC, and BSA with their possible assignments; ν is resonance frequency, γ is damping, and f is oscillator strength.

	EMF	CytC	BSA
511–560 cm^{-1}	$\nu = 532$ cm^{-1}	$\nu = 531$ cm^{-1}	$\nu = 525$ cm^{-1}
1^+–0^- transition in ν_2 vibration-inversion mode in (H$_3$O$^+$) [72]	$\gamma = 94$ cm^{-1}	$\gamma = 111$ cm^{-1}	$\gamma = 88$ cm^{-1}
	$f = 8390$ cm^{-2}	$f = 914$ cm^{-2}	$f = 92$ cm^{-2}
860–995 cm^{-1}	$\nu = 932$ cm^{-1}	$\nu = 936$ cm^{-1}	$\nu = 937$ cm^{-1}
O–H$^+$–O group vibrations in H$_5$O$_2^+$ [74]	$\gamma = 54$ cm^{-1}	$\gamma = 100$ cm^{-1}	$\gamma = 152$ cm^{-1}
	$f = 827$ cm^{-2}	$f = 925$ cm^{-2}	$f = 892$ cm^{-2}
954–1075 cm^{-1}	$\nu = 1067$ cm^{-1}	$\nu = 1029$ cm^{-1}	$\nu = 1041$ cm^{-1}
1^-–0^+ transition in (H$_3$O$^+$) ν_2 vibration-inversion mode [72]	$\gamma = 85$ cm^{-1}	$\gamma = 109$ cm^{-1}	$\gamma = 66$ cm^{-1}
	$f = 9778$ cm^{-2}	$f = 2049$ cm^{-2}	$f = 314$ cm^{-2}
1000–1160 cm^{-1}	$\nu = 1124$ cm^{-1}	$\nu = 1105$ cm^{-1}	$\nu = 1105$ cm^{-1}
ν_{as}(OHO) in H$_5$O$_2^+$ [73,74]	$\gamma = 76$ cm^{-1}	$\gamma = 74$ cm^{-1}	$\gamma = 104$ cm^{-1}
	$f = 2768$ cm^{-2}	$f = 1607$ cm^{-2}	$f = 1442$ cm^{-2}
1225–1255 cm^{-1}	$\nu = 1238$ cm^{-1}	$\nu = 1244$ cm^{-1}	$\nu = 1251$ cm^{-1}
Amide III β sheet	$\gamma = 110$ cm^{-1}	$\gamma = 84$ cm^{-1}	$\gamma = 117$ cm^{-1}
1255–1294 cm^{-1}	$f = 6386$ cm^{-2}	$f = 2570$ cm^{-2}	$f = 1991$ cm^{-2}
Amide III random coil [84]			
1292–1312 cm^{-1}	$\nu = 1313$ cm^{-1}	$\nu = 1308$ cm^{-1}	$\nu = 1308$ cm^{-1}
Amide III [84]	$\gamma = 64$ cm^{-1}	$\gamma = 95$ cm^{-1}	$\gamma = 116$ cm^{-1}
	$f = 2518$ cm^{-2}	$f = 1940$ cm^{-2}	$f = 1207$ cm^{-2}
1403–1481 cm^{-1}	$\nu = 1402$ cm^{-1}	$\nu = 1392$ cm^{-1}	$\nu = 1398$ cm^{-1}
Amide III [84]	$\gamma = 97$ cm^{-1}	$\gamma = 124$ cm^{-1}	$\gamma = 108$ cm^{-1}
	$f = 14\,286$ cm^{-2}	$f = 3375$ cm^{-2}	$f = 2253$ cm^{-2}
1597 1710 cm^{-1}	$\nu = 1650$ cm^{-1}	$\nu = 1662$ cm^{-1}	$\nu = 1662$ cm^{-1}
Amide I [53]	$\gamma = 22$ cm^{-1}	$\gamma = 176$ cm^{-1}	$\gamma = 80$ cm^{-1}
	$f = 29\,804$ cm^{-2}	$f = 6389$ cm^{-2}	$f = 3234$ cm^{-2}
~1750 cm^{-1}	$\nu = 1740$ cm^{-1}	$\nu = 1757$ cm^{-1}	$\nu = 1744$ cm^{-1}
Shared proton bend in H$_5$O$_2^+$ [82]	$\gamma = 43$ cm^{-1}	$\gamma = 15$ cm^{-1}	$\gamma = 85$ cm^{-1}
Flanking waters in H$_5$O$_2^+$ [76,81]	$f = 303$ cm^{-2}	$f = 72$ cm^{-2}	$f = 81$ cm^{-2}
2536 3010 cm^{-1}	$\nu = 2776$ cm^{-1}	$\nu = 2742$ cm^{-1}	$\nu = 2742$ cm^{-1}
O-H stretching in (H$_3$O$^+$) [75,81]	$\gamma = 384$ cm^{-1}	$\gamma = 618$ cm^{-1}	$\gamma = 539$ cm^{-1}
	$f = 29\,174$ cm^{-2}	$f = 23\,013$ cm^{-2}	$f = 9673$ cm^{-2}
~3200 cm^{-1}	$\nu = 3195$ cm^{-1}	$\nu = 3201$ cm^{-1}	$\nu = 3201$ cm^{-1}
Stretching vibrations of flanking waters in H$_5$O$_2^+$ [81,82]	$\gamma = 137$ cm^{-1}	$\gamma = 109$ cm^{-1}	$\gamma = 102$ cm^{-1}
	$f = 3594$ cm^{-2}	$f = 382$ cm^{-2}	$f = 768$ cm^{-2}
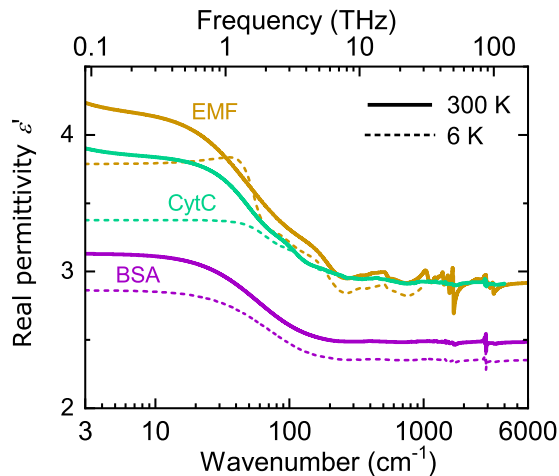
FIG. 2. Terahertz-infrared spectra of real parts of EMF, CytC, and BSA dielectric permittivity measured at 300 K (solid lines) and 5 K (dashed lines).

at 1292–1312 and 1403–1481 cm^{-1} due to the out-of- and in-plane deformations, γ(OHO) and δ(OHO), respectively. The most important feature is the ν_{as}(OHO) band at ~1000 cm^{-1} arising from SSLB H bond [34,73,74]. Also reported are the features at 1760 and 3200 cm^{-1}, related to bending and stretching vibrations of flanking water molecules, respectively [81–83]. The bands at ~930, ~1750, and 3200 cm^{-1} can be observed in the spectra of all three materials.

As for the other infrared absorption lines meeting the frequency requirements, one should treat them with caution. There are explicit bands at 1124 cm^{-1} in spectra of EMF and at 1105 cm^{-1} in spectra of CytC and BSA, which might be a result of the above-mentioned ν_{as}(OHO) vibrations. It should be noted that NH$_3^+$ rocking vibrations of amino acids' side chains are located nearby at frequencies ~1160 and ~1100 cm^{-1} [52]. However, the content of amino acid lysine, which contributes to these oscillations, is lower in EMF proteins MtrC, MtrB, MtrA, and OmcA than in CytC or BSA. This does not correlate with the corresponding peaks' intensities: the oscillator strength of the band at 1124 cm^{-1} in EMF is almost
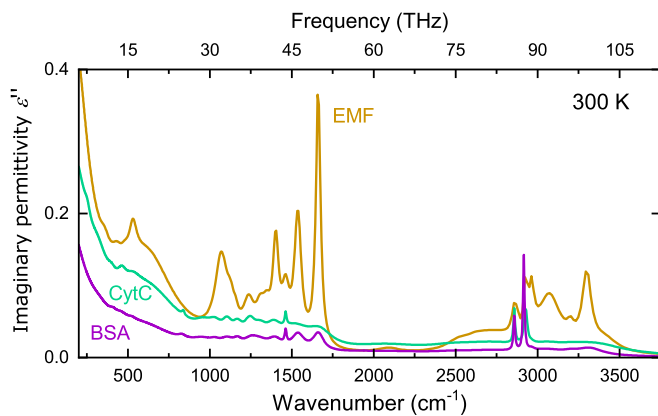
FIG. 3. Infrared spectra of the imaginary part of dielectric permittivity of EMF, CytC, and BSA measured at $T = 300\,\mathrm{K}$.

twice as large as the one of the bands at $1105\,\mathrm{cm}^{-1}$ in CytC and BSA. Shifts of lines positions of a few cm^{-1} for different biomaterials might indicate different coupling strengths of aqueous cations with the molecular environment in these materials.

Nonetheless, it is necessary to emphasize that $H_5O_2^+$ $\nu_{as}(OHO)$ vibration and H_3O^+ ν_2 vibration-inversion bands are still quite hard to discern because of their proximity. The differentiation problem remains the same at higher frequencies, where the region of interest for studying aqueous cations' response overlaps with the regions of infrared activity of protein residues. The Zundel ion $\gamma(OHO)$ and $\delta(OHO)$ weak vibrations can hardly be observed in our samples due to proteins' amide III vibrational bands at 1295–$1320\,\mathrm{cm}^{-1}$ (α helix) and multiple lines of amino acid side chains within the range 1375–$1480\,\mathrm{cm}^{-1}$ [53,84]. The line at 1672–$1700\,\mathrm{cm}^{-1}$ could also be a part of a complex absorption landscape in that spectral region, together with the $\delta_{as}(H_3O^+)$ band of hydronium, but discerning them from amide I band is also fraught with difficulties. The same applies to H_3O^+ umbrella bending mode at $1250\,\mathrm{cm}^{-1}$ [76] and amide III β-sheet and random coil bands, at 1225–1255 and 1255–$1294\,\mathrm{cm}^{-1}$, respectively [84].

All the above-mentioned absorption lines with their parameters and possible origin are summarized in Table I.

IV. DISCUSSION

Considering the data of Table I and Figs. 3 and 4, one can see that the absorption bands related to the response of hydronium ion (or Eigen ion regarded as hydronium ion bound by three molecules of water via hydrogen bonds) are markedly more intense in EMF than in CytC and even more so than in BSA. The same is true for almost all the bands related to the Zundel ion vibrations, with the latter being orders of magnitude less intense in EMF than the bands detected for hydronium. Assuming that the molar absorption coefficient of the hydronium and Zundel ions is approximately the same in all three protein systems, we come to the following conclusions. First, the content of hydronium ions is reduced significantly in CytC compared to EMF, and it is even smaller in BSA. Second, the amount of H_3O^+ cations
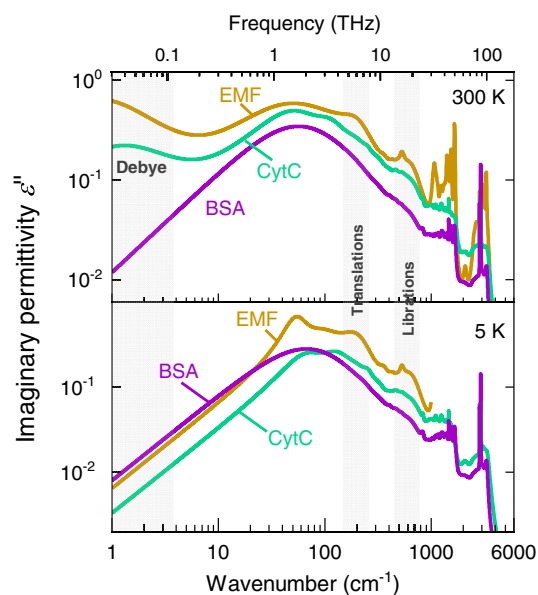
FIG. 4. Terahertz-infrared spectra of imaginary parts of dielectric permittivity of EMF, CytC, and BSA samples measured at 300 and 5 K. "Debye" indicates the subterahertz part of the spectra where a Debye-type relaxational response of bound water is detected in the spectra of EMF and CytC. In the infrared range, frequency intervals are indicated where translational (T) and librational (L) vibrations of H_2O molecules are observed.

in EMF prevails over that of $H_5O_2^+$. One notes the curious correlation with the results of our previous studies [48], where we have observed free-carrier (Drude-like) conductivity in EMF to be orders of magnitude greater than that in CytC, and no delocalized charge carriers to be present in the BSA samples despite being equal with CytC hydration level. The rise of conductivity values correlated with the strengthening of response due to bound water absorption of the samples in the subterahertz range (Fig. 4). The situation prompts us to consider the current knowledge about the relation between the concentration ratio $H_3O^+/H_5O_2^+$ and the level of proton conductivity in well-studied systems. Solid heteropolyacids can be taken as the first example. Among them, the Keggin-type 12 tungstophosphoric acid (TPA, $H_3PW_{12}O_{40} \times H_2O_n$, where $0 \leqslant n \leqslant 24$ is a controllable parameter) is of particular interest due to its chemical stability and the strongest acidity, and, as a consequence, well-studied structure and electrical conductivity at different levels of hydration. In this system, proton mobility negatively correlates with the prevalence of $H_5O_2^+$ cation among the other hydrated proton forms [38]. Dissipation of $H_5O_2^+$ due to increase or decrease of water concentration leads to the formation of labile hydronium or Eigen cations. The interested reader can get acquainted with detailed studies of this issue utilizing QENS [85,86], NMR [38,39,41–43,87], and other techniques [44,88] in the corresponding references.

The second example is the so-called floating water bridge observed when a high ($\sim$ kV cm^{-1}) potential difference is applied between two beakers of any polar liquid with low conductivity [89–91]. Induced by the field, the liquid jumps to the edges of the beakers and forms a free-hanging elastic

flow connecting the two volumes. The effect was first reported by Sir William Armstrong in 1893 but forgotten for several decades [92]. However, in recent years, it has been studied in detail by several groups that have been able to identify several remarkable features of the phenomenon. Teschke *et al.* demonstrated that the Raman spectrum of the bridge could be modeled by a superposition of Zundel and Eigen cations spectra [93]. Zundel-like contribution prevailed at a voltage of 6.3 kV. As the applied voltage increased, the Eigen-like spectral contribution added to the overall spectral feature. There is no surprise since Zundel cation is the simplest stable proton hydrate [35]. High concentrations of (H_3O^+) are achievable only under special conditions, i.e., high concentration of a strong acid and low water concentration [35,78]. Otherwise, the equilibrium $H_3O^+ + H_2O \rightleftarrows H_5O_2^+$ is strongly shifted to the right. Higher voltages lead to the faster synthesis of protons on the anode and, consequently, to the local insufficiency of water molecules needed to hydrate hydronium cations into Zundel cations. In this way, the relations between conductivity and the prevalence of Zundel cation are similar in the floating bridge, variously hydrated TPA, and the studied proteins. In another study, Teschke *et al.* [94] demonstrated that the increase of voltage-dependent proton current in the bridge corresponds to the growth of the intensity of water molecular translational vibrations. Again, as in EMF and CytC, the increased intensity of translations corresponds to greater conductivity values measured in the radiofrequency range.

The physics behind the floating water bridge phenomenology is still a matter of intensive study. However, important strides have been made recently in developing the general theory of the phenomenon. The enhanced mobility of protons in the bridge is associated with the formation of proton channels [95]. The latter is supposed to be caused by the symmetry breaking of the water structure revealed by the applied electrical field. Namely, water is prone to topological changes [96]. The presence of a high electric field as a mandatory condition for higher charge mobility was articulated more than 60 years ago [97]. Neither molecular dynamics simulations nor electrohydrodynamic flow simulations are sufficient to explain various microscopic effects observed in the experiments [95,98,99]. To solve the problem, Fuchs *et al.*, in their recent article [91], appeal to the terms of Landau's theory of phase transitions and persuasively represent the floating bridge as an example of a dynamic second-order phase transition. The interested reader should refer to this remarkable series of works.

Are those high electric fields needed for the floating bridges relevant to biological systems? Yes, they are. Cellular power stations, i.e., mitochondria, responsible for the synthesis of adenosine triphosphate (ATP) during oxidative phosphorylation, support electrochemical transmembrane potentials with values up to 150 millivolts per 5 nanometers, i.e., 3×10^7 V/m. Previously, it was thought that the electrostatic field that arises at the inner mitochondrial membrane is effectively shielded and does not penetrate over long distances deep into the cytosol. The development of nanosized supramolecular voltmeters [100] demonstrated that high electrical fields, sufficient for establishing a floating water bridge on a macroscopic level, are found in the whole cytosol. In mitochondria, the transmembrane hydrodynamics may play

an important role for ATP synthase molecular machine, which probably functions as a watermill utilizing the flow of the field-accelerated proton cations to synthesize ATP. Unfortunately, the structure of the pathway the protons take through the membrane domain of ATP synthase is known presently with low spatial resolution, of only 4 Å [101,102]. For this reason, we cannot judge confidently in what form the proton (H^+ or H_3O^+) enters the enzyme and performs its function, or, in other words, whether the hydronium cation decays into the water molecule and a proton in the membrane domain or not.

There exist limited data on water dynamics in the first hydration layer of the mitochondrial membrane. However, we know that mobile proton species in the intermembrane space of mitochondria can be divided into two main types even at the current level of our knowledge. The first type is associated with the mechanism of localized coupling of respiration and phosphorylation postulated by Williams in 1961 [103]. These charges are less hydrated, coupled with the membrane surface, and are directly consumed for ATP synthesis [104]. Due to their relative thermodynamic instability, these charges can be extracted into the bulk phase in intermembrane space utilizing catalysts like 4-(2-hydroxyethyl)-1-piperazineethanesulfonic acid (HEPES) [105]. The specific uncouplers with hydrophobic anchors can selectively transfer them back into the mitochondrial matrix and uncouple the inner mitochondrial membrane [106]. We tend to associate these membrane interfacial protons with hydronium cations due to interfacial localization and additional free energy compared to the charges in the bulk phase. The second type of proton species are those in the bulk phase; these are, presumably, more stable and less mobile Zundel-like cations.

CytC and EMF contain membrane and membrane-associated proteins responsible for the corresponding cellular energetics, which includes electron transport and support of transmembrane electrochemical proton potential. Therefore, similar spectral features observed in these materials and the efficient proton conductors like TPA and floating bridge are no surprise. Moreover, theoretical electrohydrodynamic approaches developed to explain the floating bridge phenomenon may bring insights to understanding the functioning of ATP-synthase and the whole supercomplex of membrane enzymes forming the oxidative phosphorylation machinery (so-called OXPHOS). We may suppose that enhanced dielectric contribution of translational vibrations of water molecules even without strong external electrostatic fields observed in membrane and membrane-associated proteins in CytC and EMF features the preformation of interfacial water that can promote enhanced proton transportation. In some cases, ATP synthase can also be located at the external membrane of *S. oneidensis* [107].

It is important to add that experimental detection of aqueous cations in the samples may be regarded as evidence of the excess protons present within the bulk of the material. However, bound water itself and bound aqueous proton cations do not necessarily indicate the availability of effective proton transport. For example, there is a transfer of water molecules in the aquaporin channel. Still, the electrostatic barrier does not allow hydronium ions to move into the channel from the outside, and protons do not enter the cell [108]. Another

structural prerequisite for the lack of charge transport may be the failure of the hydration network to cross the percolation threshold, for example, due to the shape of the protein surface. Significant differences in the conductivity values in EMF, CytC, and BSA can be due to the different structures of these biomaterials. Percolation water networks inside them can be organized in different ways. The absence of the Debye contribution in the subterahertz part of the spectrum in the case of BSA suggests that water, at formally equal concentrations in BSA and CytC, is more strongly bound in BSA molecular environment. Hydration networks in BSA might not overcome the percolation threshold required for proton transport over relatively long distances. We also see that the librational modes in the BSA spectra have a larger dielectric contribution than the translational ones. Bound water is in a more localized state, and no free-carrier conductivity is observed [48].

Although we do not know which structures water forms in our samples, and the terahertz-infrared dielectric response of the hydration shell is almost impossible to measure, there still exist some clues to understand how water layers are organized. In the spectra of all the three samples in Fig. 4, a broad and intense band at 50 cm^{-1} is observed. There are hypotheses about its origin, including relating this band to long-range protein vibrations [109], or to the O-O-O bending mode of polygonal water clusters, which often form at the surfaces and in the voids of different proteins [31,110]. However, the precise determination of this band nature requires more research.

The presence of hydronium ions is usually directly related to excess protons in the system. Therefore, the signs of hydronium and other aqueous cations found in the studied biomaterials can indirectly indicate the type of charge transport there. Yet when talking about aqueous cations, it is essential to keep in mind that they are difficult to distinguish from one another, and the research on aqueous protons in condensed media is far from complete. We regard the prevalence of aqueous translations in THz/FIR (far-infrared) range as a stronger argument towards excess of mobile protons in EMF and CytC than features of intramolecular vibrations attributed to H_3O^+ and $H_5O_2^+$ detected at higher frequencies.

It is also important to note that neutral and slightly acidic pH values keep CytC positively charged (pI$_{CytC}$ above 9.5) and BSA negatively charged (pI$_{BSA}$ below 5.2) [111]. Thus, CytC from industrial packaging should be a complex cation (alkylammonium/imidazole–guanidine), binding hydroxyls and freeing proton cations in water. BSA is an anion (with sodium counterions in our case [48]) and should accept protons from water producing hydroxyls. The latter can partially explain an excess of aqueous proton cations in the case of CytC sample. In its turn, EMF should represent a complex of many proteins with isoelectric points lying in a range from about 8.5 for CymA to about 4.5 for MtrB. Since EMF contained more water and the ratio between its protein components remained unknown, it is more logical to regard it as a separate case and do not include CytC and BSA in comparison [48].

Interestingly, the NMR data for CytC and BSA [112,113] demonstrate some interrelationship with our results. Various attempts to estimate rigidly bound waters per molecule gave numbers from 25 to 60 for BSA [113,114] and from 2 to 4 for CytC [112,115]. It means that the same hydration levels lead to quite different ratios between strongly bound and relatively free water molecules for these two systems. BSA has a more developed surface with cavities in which water should persist in a more fixed state. Indirectly we observed another possible consequence of this effect in specific heat as a feature near 170 K [48], where the caged water may freeze.

V. CONCLUSION

In this paper, another attempt was made to illustrate the effect of bound water and aqueous cations on charge transport in three biological systems: *S. oneidensis* MR-1 extracellular matrix and filaments, and proteins cytochrome c and bovine serum albumin. Spectral signatures of H_3O^+ and $H_5O_2^+$ species observed in the samples' infrared transmittance and reflectance spectra indicate the presence of aqueous proton cations in all three materials. The characteristics of aqueous cations absorption bands allow us to judge with a considerable degree of certainty that the excess protons' content is much higher in EMF samples than in CytC and is the lowest in BSA, which correlates with the electrical conductivity values in these materials. The free-carrier conductivity in EMF was observed to be orders of magnitude greater than in CytC, but no evidence of charge transport was detected in BSA. Such correlation in the behavior of delocalized charge carriers and the presence of aqueous cations suggests that aqueous proton cations are the main charge carriers within the studied biological materials. Finally, the presence of these cations' absorption lines in the infrared spectra of biological materials might potentially serve as an additional sign of their ability to transport electrical charge. Some of the frequently used spectral signatures of excess protons in materials do not work well in proteins because of the proximity of the intense contributions of vibrational protein residues, such as amide bands. However, infrared lines at 530 and ∼1000 cm^{-1}, together with the Debye subterahertz relaxation and translational vibrations at 200 cm^{-1}, can be considered as a good indicator of the presence of proton transport in the biomaterials EMF and CytC, as confirmed by the correlations discussed in this work.

[1] J. Q. Boedicker, M. Gangan, K. Naughton, F. Zhao, J. A. Gralnick, and M. Y. El-Naggar, Engineering biological electron transfer and redox pathways for nanoparticle synthesis, Bioelectr. **3**, 126 (2021).

[2] D. R. Lovley and J. Yao, Intrinsically conductive microbial nanowires for 'Green' electronics with novel functions, Trends Biotechnol. **39**, 940 (2021).

[3] N. A. of Engineering, *Grand Challenges for Engineering: Imperatives, Prospects, and Priorities: Summary of a Forum* (The National Academies Press, Washington, DC, 2016).

[4] M. Sheliakina, A. B. Mostert, and P. Meredith, An all-solid-state biocompatible ion-to-electron transducer for bioelectronics, Mater. Horiz. **5**, 256 (2018).

[5] Y. Wang, H. Wang, J. Xuan, and D. Y. C. Leung, Powering future body sensor network systems: A review of power sources, Biosens. Bioelectron. **166**, 112410 (2020).

[6] D. Wang, J. Tan, H. Zhu, Y. Mei, and X. Liu, Biomedical implants with charge-transfer monitoring and regulating abilities, Adv. Sci. **8**, 2004393 (2021).

[7] I. Willner and E. Katz (eds.), *Bioelectronics: From Theory to Applications* (Wiley-VCH, Weinheim, 2005).

[8] R. Sarpeshkar, *Ultra Low Power Bioelectronics: Fundamentals, Biomedical Applications, and Bio-Inspired Systems, 1st ed.* (Cambridge University Press, Cambridge, UK, New York, 2010).

[9] S. Carrara and K. Iniewski, *Handbook of Bioelectronics: Directly Interfacing Electronics and Biological Systems,* 1st ed. (Cambridge University Press, Cambridge, UK, 2015).

[10] *Dielectric Relaxation in Biological Systems: Physical Principles, Methods, and Applications*, edited by V. Raicu and Y. Feldman (Oxford University Press, Oxford, 2015).

[11] A. Garcia-Etxarri and R. Yuste, Time for nanoneuro, Nat. Methods **18**, 1287 (2021).

[12] R. C. G. Creasey, A. B. Mostert, T. A. H. Nguyen, B. Virdis, S. Freguia, and B. Laycock, Microbial nanowires – electron transport and the role of synthetic analogues, Acta Biomater. **69**, 1 (2018).

[13] K. Michaeli, D. N. Beratan, D. H. Waldeck, and R. Naaman, Voltage-induced long-range coherent electron transfer through organic molecules, Proc. Natl. Acad. Sci. **116**, 5931 (2019).

[14] Y. Yang, Z. Wang, C. Gan, L. H. Klausen, R. Bonné, G. Kong, D. Luo, M. Meert, C. Zhu, G. Sun, J. Guo, Y. Ma, J. T. Bjerg, J. Manca, M. Xu, L. P. Nielsen, and M. Dong, Long-distance electron transfer in a filamentous Gram-positive bacterium, Nat. Commun. **12**, 1709 (2021).

[15] P. Meredith, C. J. Bettinger, M. Irimia-Vladu, A. B. Mostert, and P. E. Schwenn, Electronic and optoelectronic materials and devices inspired by nature, Rep. Prog. Phys. **76**, 034501 (2013).

[16] V. Forti, C. P. Baldé, R. Kuehr, and G. Bel, *The Global E-Waste Monitor 2020: Quantities, Flows and the Circular Economy Potential* (United Nations University (UNU)/United Nations Institute for Training and Research (UNITAR) – co-hosted SCYCLE Programme, International Telecommunication Union (ITU) & International Solid Waste Association (ISWA), Bonn/Geneva/Rotterdam, 2021).

[17] M. Irimia-Vladu, "Green" electronics: Biodegradable and biocompatible materials and devices for sustainable future, Chem. Soc. Rev. **43**, 588 (2013).

[18] N. Ashkenasy, W. S. Horne, and M. R. Ghadiri, Design of self-assembling peptide nanotubes with delocalized electronic states, Small **2**, 99 (2006).

[19] K. Tao, P. Makam, R. Aizen, and E. Gazit, Self-assembling peptide semiconductors, Science **358**, eaam9756 (2017).

[20] S. M. M. Reddy, E. Raßlenberg, S. Sloan-Dennison, T. Hesketh, O. Silberbush, T. Tuttle, E. Smith, D. Graham, K. Faulds, R. V. Ulijn, N. Ashkenasy, and A. Lampel, Proton-conductive melanin-like fibers through enzymatic oxidation of a self-assembling peptide, Adv. Mater. **32**, 2003511 (2020).

[21] R. Misra, S. Rudnick-Glick, and L. Adler-Abramovich, From folding to assembly: Functional supramolecular architectures of peptides comprised of non-canonical amino acids, Macromol. Biosci. **21**, 2100090 (2021).

[22] A. Handelman, P. Beker, N. Amdursky, and G. Rosenman, Physics and engineering of peptide supramolecular nanostructures, Phys. Chem. Chem. Phys. **14**, 6391 (2012).

[23] A. B. Mostert, Melanin, the what, the why and the how: An introductory review for materials scientists interested in flexible and versatile polymers, Polymers **13**, 10 (2021).

[24] J.-L. Mergny and D. Sen, DNA quadruple helices in nanotechnology, Chem. Rev. **119**, 6290 (2019).

[25] A. B. Mostert, S. B. Rienecker, M. Sheliakina, P. Zierep, G. R. Hanson, J. R. Harmer, G. Schenk, and P. Meredith, Engineering proton conductivity in melanin using metal doping, J. Mater. Chem. B **8**, 8050 (2020).

[26] M. Amit, S. Appel, R. Cohen, G. Cheng, I. W. Hamley, and N. Ashkenasy, Hybrid proton and electron transport in peptide fibrils, Adv. Funct. Mater. **24**, 5873 (2014).

[27] S. Khodadadi, S. Pawlus, and A. P. Sokolov, Influence of hydration on protein dynamics: Combining dielectric and neutron scattering spectroscopy data, J. Phys. Chem. B **112**, 14273 (2008).

[28] A. Grebenko, V. Dremov, P. Barzilovich, A. Bubis, K. Sidoruk, T. Voeikova, Z. Gagkaeva, T. Chernov, E. Korostylev, B. Gorshunov, and K. Motovilov, Impedance spectroscopy of single bacterial nanofilament reveals water-mediated charge transfer, PLoS ONE **13**, e0191289 (2018).

[29] A. B. Mostert, B. J. Powell, F. L. Pratt, G. R. Hanson, T. Sarna, I. R. Gentle, and P. Meredith, Role of semiconductivity and ion transport in the electrical conduction of melanin, Proc. Natl. Acad. Sci. **109**, 8943 (2012).

[30] K. Sasaki, I. Popov, and Y. Feldman, Water in the hydrated protein powders: Dynamic and structure, J. Chem. Phys. **150**, 204504 (2019).

[31] J. Lee and S.-H. Kim, Water polygons in high-resolution protein crystal structures, Protein Sci. **18**, 1370 (2009).

[32] F. Garczarek, L. S. Brown, J. K. Lanyi, and K. Gerwert, Proton binding within a membrane protein by a protonated water cluster, Proc. Natl. Acad. Sci. **102**, 3633 (2005).

[33] J. A. Martinez-Gonzalez, H. Cavaye, J. D. McGettrick, P. Meredith, K. A. Motovilov, and A. B. Mostert, Interfacial water morphology in hydrated melanin, Soft Matter **17**, 7940 (2021).

[34] C. A. Reed, Myths about the proton. The nature of H+ in condensed media, Acc. Chem. Res. **46**, 2567 (2013).

[35] M. V. Vener and N. B. Librovich, The structure and vibrational spectra of proton hydrates: As a simplest stable ion, Int. Rev. Phys. Chem. **28**, 407 (2009).

[36] M. V. Vener, I. Yu. Chernyshov, A. A. Rykounov, and A. Filarowski, Structural and spectroscopic features of proton hydrates in the crystalline state. Solid-state DFT study on HCl and triflic acid hydrates, Mol. Phys. **116**, 251 (2018).

[37] G. V. Yukhnevich, E. G. Tarakanova, V. D. Maiorov, and N. B. Librovich, The structure and vibrational spectra of proton solvates in solution, Russ. Chem. Rev. **64**, 901 (1995).

[38] D. I. Kolokolov, M. S. Kazantsev, M. V. Luzgin, H. Jobic, and A. G. Stepanov, Characterization and dynamics of the different protonic species in hydrated 12-Tungstophosphoric acid studied by 2H NMR, J. Phys. Chem. C **118**, 30023 (2014).

[39] D. I. Kolokolov, M. S. Kazantsev, M. V. Luzgin, H. Jobic, and A. G. Stepanov, Direct 2H NMR observation of the proton mobility of the acidic sites of anhydrous 12-Tungstophosphoric acid, ChemPhysChem **14**, 1783 (2013).

[40] P. Colomban, Proton conductors and their applications: A tentative historical overview of the early researches, Solid State Ionics **334**, 125 (2019).

[41] M. de Oliveira, U. P. Rodrigues-Filho, and J. Schneider, Thermal transformations and proton species in 12-Phosphotungstic acid hexahydrate studied by 1H and 31P solid-state nuclear magnetic resonance, J. Phys. Chem. C **118**, 11573 (2014).

[42] S. Uchida, K. Inumaru, and M. Misono, States and dynamic behavior of protons and water molecules in H3PW12O40 pseudoliquid phase analyzed by solid-state MAS NMR, J. Phys. Chem. B **104**, 8108 (2000).

[43] S. Uchida, K. Inumaru, J. M. Dereppe, and M. Misono, The first direct detection of rapid migration of acidic protons between heteropolyanions in $H_3PW_{12}O_{40} \cdot nH_2O$ (n < 6) by ^{31}P NMR, Chem. Lett. **27**, 643 (1998).

[44] D. J. Jones and J. Rozière, Complementarity of optical and incoherent inelastic neutron scattering spectroscopies in the study of proton conducting materials, Solid State Ionics **61**, 13 (1993).

[45] Y. Gu, V. Srikanth, A. I. Salazar-Morales, R. Jain, J. P. O'Brien, S. M. Yi, R. K. Soni, F. A. Samatey, S. E. Yalcin, and N. S. Malvankar, Structure of *geobacter* pili reveals secretory rather than nanowire behaviour, Nature (London) **597**, 430 (2021).

[46] S. Pirbadian, M. S. Chavez, and M. Y. El-Naggar, Spatiotemporal mapping of bacterial membrane potential responses to extracellular electron transfer, Proc. Natl. Acad. Sci. **117**, 20171 (2020).

[47] Z. V. Gagkaeva, E. S. Zhukova, V. Grinenko, A. K. Grebenko, K. V. Sidoruk, T. A. Voeikova, M. Dressel, and B. P. Gorshunov, Terahertz-infrared spectroscopy of Shewanella oneidensis MR-1 extracellular matrix, J. Biol. Phys. **44**, 401 (2018).

[48] K. A. Motovilov, M. Savinov, E. S. Zhukova, A. A. Pronin, Z. V. Gagkaeva, V. Grinenko, K. V. Sidoruk, T. A. Voeikova, P. Yu. Barzilovich, A. K. Grebenko, S. V. Lisovskii, V. I. Torgashev, P. Bednyakov, J. Pokorný, M. Dressel, and B. P. Gorshunov, Observation of dielectric universalities in albumin, Cytochrome C and Shewanella oneidensis MR-1 extracellular matrix, Sci. Rep. **7**, 15731 (2017).

[49] A. V. Sokolov, *Optical Properties of Metals*, 1st ed. (American Elsevier Publishing Co., New York, 1967).

[50] I. Popov, P. B. Ishai, A. Khamzin, and Y. Feldman, The mechanism of the dielectric relaxation in water, Phys. Chem. Chem. Phys. **18**, 13941 (2016).

[51] P. Subramanian, S. Pirbadian, M. Y. El-Naggar, and G. J. Jensen, Ultrastructure of Shewanella oneidensis MR-1 nanowires revealed by electron cryotomography, Proc. Natl. Acad. Sci. **115**, E3246 (2018).

[52] S. Krimm and J. Bandekar, in *Advances in Protein Chemistry*, edited by C. B. Anfinsen, J. T. Edsall, and F. M. Richards, Vol. 38 (Academic Press, New York, London, 1986), pp. 181–364.

[53] A. Barth, Infrared spectroscopy of proteins, Biochim. Biophys. Acta BBA - Bioenerg. **1767**, 1073 (2007).

[54] C. Kittel, *Introduction to Solid State Physics*, 8th ed. (Wiley, Hoboken, NJ, 2005).

[55] N. Ashcroft and D. Mermin, *Solid State Physics* (Saunders College Publishing, Belmont, California, 1976).

[56] N. F. Mott and E. A. Davis, *Electronic Processes in Non-Crystalline Materials* (Oxford University Press, London, 1971).

[57] F. Ciucci, Modeling electrochemical impedance spectroscopy, Curr. Opin. Electrochem. **13**, 132 (2019).

[58] R. Hempelmann, *Quasielastic Neutron Scattering and Solid State Diffusion* (Clarendon Press, Oxford, 2000).

[59] E. O. Stejskal and J. E. Tanner, Spin diffusion measurements: Spin echoes in the presence of a time-dependent field gradient, J. Chem. Phys. **42**, 288 (1965).

[60] V. I. Volkov, A. V. Chernyak, I. A. Avilova, N. A. Slesarenko, D. L. Melnikova, and V. D. Skirda, Molecular and ionic diffusion in ion exchange membranes and biological systems (cells and proteins) Studied by NMR, Membranes **11**, 6 (2021).

[61] *Muon Spectroscopy: An Introduction*, edited by S. J. Blundell, R. D. Renzi, T. Lancaster, and F. L. Pratt (Oxford University Press, New York, 2022).

[62] M. Amit, S. Roy, Y. Deng, E. Josberger, M. Rolandi, and N. Ashkenasy, Measuring proton currents of bioinspired materials with metallic contacts, ACS Appl. Mater. Interfaces **10**, 1933 (2018).

[63] M. Reali, P. Saini, and C. Santato, Electronic and protonic transport in bio-sourced materials: A new perspective on semiconductivity, Mater. Adv. **2**, 15 (2021).

[64] A. Bernardus Mostert, B. J. Powell, I. R. Gentle, and P. Meredith, On the origin of electrical conductivity in the bioelectronic material melanin, Appl. Phys. Lett. **100**, 093701 (2012).

[65] H. Chen and J. F. Stoddart, From molecular to supramolecular electronics, Nat. Rev. Mater. **6**, 804 (2021).

[66] A. Grebenko, A. Bubis, K. Motovilov, V. Dremov, E. Korostylev, I. Kindiak, F. S. Fedorov, S. Luchkin, Y. Zhuikova, A. Trofimenko, G. Filkov, G. Sviridov, A. Ivanov, J. T. Dull, R. Mozhchil, A. Ionov, V. Varlamov, B. P. Rand, V. Podzorov, and A. G. Nasibulin, Green lithography for delicate materials, Adv. Funct. Mater. **31**, 2101533 (2021).

[67] A. I. González Flórez, E. Mucha, D.-S. Ahn, S. Gewinner, W. Schöllkopf, K. Pagel, and G. von Helden, Charge-induced unzipping of isolated proteins to a defined secondary structure, Angew. Chem. Int. Ed. **55**, 3295 (2016).

[68] J. Oomens, N. Polfer, D. T. Moore, L. van der Meer, A. G. Marshall, J. R. Eyler, G. Meijer, and G. von Helden, Charge-state resolved mid-infrared spectroscopy of a gasphase protein, Phys. Chem. Chem. Phys. **7**, 1345 (2005).

[69] D. Moss, E. Nabedryk, J. Breton, and W. Mäntele, Redoxlinked conformational changes in proteins detected by a

combination of infrared spectroscopy and protein electrochemistry, Eur. J. Biochem. **187**, 565 (1990).

[70] M. Jackson and H. H. Mantsch, The use and misuse of FTIR spectroscopy in the determination of protein structure, Crit. Rev. Biochem. Mol. Biol. **30**, 95 (1995).

[71] J. Grdadolnik and Y. Maréchal, Bovine serum albumin observed by infrared spectrometry. II. Hydration mechanisms and interaction configurations of embedded H2O molecules, Biopolymers **62**, 54 (2001).

[72] D. Liu, N. N. Haese, and T. Oka, Infrared spectrum of the N2 vibration-inversion band of H3O+, J. Chem. Phys. **82**, 5368 (1985).

[73] E. S. Stoyanov, I. V. Stoyanova, and C. A. Reed, The structure of the hydrogen ion (Haq+) in water, J. Am. Chem. Soc. **132**, 1484 (2010).

[74] E. S. Stoyanov and C. A. Reed, IR spectrum of the H_5O^{2+} cation in the context of proton disolvates $L-H^+-L$, J. Phys. Chem. A **110**, 12992 (2006).

[75] E. S. Stoyanov, K.-C. Kim, and C. A. Reed, The nature of the H3O+ hydronium ion in benzene and chlorinated hydrocarbon solvents. Conditions of existence and reinterpretation of infrared data, J. Am. Chem. Soc. **128**, 1948 (2006).

[76] R. Biswas, W. Carpenter, J. A. Fournier, G. A. Voth, and A. Tokmakoff, IR spectral assignments for the hydrated excess proton in liquid water, J. Chem. Phys. **146**, 154507 (2017).

[77] G. Zundel, Hydrate structures, intermolecular interactions and proton conducting mechanism in polyelectrolyte membranes — infrared results, J. Membr. Sci. **11**, 249 (1982).

[78] F. Dahms, R. Costard, E. Pines, B. P. Fingerhut, E. T. J. Nibbering, and T. Elsaesser, The hydrated excess proton in the Zundel cation H5O2+: The role of ultrafast solvent fluctuations, Angew. Chem. Int. Ed. **55**, 10600 (2016).

[79] F. Dahms, B. P. Fingerhut, E. T. J. Nibbering, E. Pines, and T. Elsaesser, Large-amplitude transfer motion of hydrated excess protons mapped by ultrafast 2D IR spectroscopy, Science **357**, 491 (2017).

[80] A. Kundu, F. Dahms, B. P. Fingerhut, E. T. J. Nibbering, E. Pines, and T. Elsaesser, Hydrated excess protons in acetonitrile/water mixtures: Solvation species and ultrafast proton motions, J. Phys. Chem. Lett. **10**, 2287 (2019).

[81] M. Thämer, L. D. Marco, K. Ramasesha, A. Mandal, and A. Tokmakoff, Ultrafast 2D IR spectroscopy of the excess proton in liquid water, Science **350**, 78 (2015).

[82] N. Heine, M. R. Fagiani, M. Rossi, T. Wende, G. Berden, V. Blum, and K. R. Asmis, Isomer-selective detection of hydrogen-bond vibrations in the protonated water hexamer, J. Am. Chem. Soc. **135**, 8266 (2013).

[83] J. Kim, U. W. Schmitt, J. A. Gruetzmacher, G. A. Voth, and N. E. Scherer, The vibrational spectrum of the hydrated proton: Comparison of experiment, simulation, and normal mode analysis, J. Chem. Phys. **116**, 737 (2002).

[84] B. R. Singh, D. B. DeOliveira, F.-N. Fu, and M. P. Fuller, in *Biomolecular Spectroscopy III*, Vol. 1890 (SPIE, 1993), pp. 47–55.

[85] R. C. T. Slade, G. P. Hall, H. A. Pressman, and I. M. Thompson, Reorientational motions of hydrogenic species in 12-Tungstophosphoric acid 14-Hydrate: A neutron scattering study, J. Mater. Chem. **1**, 685 (1991).

[86] H. A. Pressman and R. C. T. Slade, Internal rotation in the H5O2+ ion: A quasielastic neutron scattering study of 12-Tungstophosphoric acid hexahydrate, Chem. Phys. Lett. **151**, 354 (1988).

[87] R. C. T. Slade, J. Barker, and H. A. Pressman, Studies of protonic self-diffusion and conductivity in 12-Tungstophosphoric acid hydrates by pulsed field gradient 1H NMR and AC conductivity, Solid State Ion. **28–30**, 594 (1988).

[88] U. Mioč, M. Davidović, N. Tjapkin, Ph. Colomban, and A. Novak, Equilibrium of the protonic species in hydrates of some heteropolyacids at elevated temperatures, Solid State Ion. **46**, 103 (1991).

[89] J. Woisetschläger, A. D. Wexler, G. Holler, M. Eisenhut, K. Gatterer, and E. C. Fuchs, Horizontal bridges in polar dielectric liquids, Exp. Fluids **52**, 193 (2012).

[90] E. C. Fuchs, D. Yntema, and J. Woisetschläger, Raman spectroscopy and shadowgraph visualization of excess protons in high-voltage electrolysis of pure water, J. Phys. Appl. Phys. **52**, 365302 (2019).

[91] E. C. Fuchs, J. Woisetschläger, A. D. Wexler, R. Pecnik, and G. Vitiello, Electrically induced liquid–liquid phase transition in a floating water bridge identified by refractive index variations, Water **13**, 5 (2021).

[92] W. G. Armstrong, The Newcastle Literary and Philosophical Society, Electr. Eng., 154 (1893).

[93] O. Teschke, J. R. de Castro, J. F. Valente Filho, and D. M. Soares, Protonic charge defect structures in floating water bridges observed as Zundel and Eigen solvation arrangements, Chem. Phys. Lett. **685**, 239 (2017).

[94] O. Teschke, J. R. Castro, and D. M. Soares, Translational vibration modes—the spectral signature of excess proton transport in water, Phys. Fluids **30**, 112104 (2018).

[95] E. C. Fuchs, B. Bitschnau, A. D. Wexler, J. Woisetschläger, and F. T. Freund, A quasi-elastic neutron scattering study of the dynamics of electrically constrained water, J. Phys. Chem. B **119**, 15892 (2015).

[96] A. D. Wexler, E. C. Fuchs, J. Woisetschläger, and G. Vitiello, Electrically induced liquid–liquid phase transition in water at room temperature, Phys. Chem. Chem. Phys. **21**, 18541 (2019).

[97] O. M. Stuetzer, Magnetohydrodynamics and electrohydrodynamics, Phys. Fluids **5**, 534 (1962).

[98] L. Piatkowski, A. D. Wexler, E. C. Fuchs, H. Schoenmaker, and H. J. Bakker, Ultrafast vibrational energy relaxation of the water bridge, Phys. Chem. Chem. Phys. **14**, 6160 (2012).

[99] A. D. Wexler, S. Drusová, J. Woisetschläger, and E. C. Fuchs, Non-equilibrium thermodynamics and collective vibrational modes of liquid water in an inhomogeneous electric field, Phys. Chem. Chem. Phys. **18**, 16281 (2016).

[100] K. M. Tyner, R. Kopelman, and M. A. Philbert, "Nanosized voltmeter" enables cellular-wide electric field mapping, Biophys. J. **93**, 1163 (2007).

[101] E. Morales-Rios, M. G. Montgomery, A. G. W. Leslie, and J. E. Walker, Structure of ATP synthase from paracoccus denitrificans determined by X-ray crystallography at 4.0 Å resolution, Proc. Natl. Acad. Sci. **112**, 13231 (2015).

[102] P. Peck, *The Structure and Function of ATP Synthases*, https://www.mrc-mbu.cam.ac.uk/research-groups/walker-group/structure-and-function-atp-synthases.

[103] R. J. P. Williams, Possible functions of chains of catalysts, J. Theor. Biol. **1**, 1 (1961).

[104] L. S. Yaguzhinsky, V. I. Yurkov, and I. P. Krasinskaya, On the localized coupling of respiration and phosphorylation in mitochondria, Biochim. Biophys. Acta BBA - Bioenerg. **1757**, 408 (2006).

[105] V. S. Moiseeva, K. A. Motovilov, N. V. Lobysheva, V. N. Orlov, and L. S. Yaguzhinsky, The formation of metastable bond between protons and mitoplast surface, Dokl. Biochem. Biophys. **438**, 127 (2011).

[106] K. A. Motovilov, V. I. Yurkov, E. M. Volkov, and L. S. Yaguzhinsky, Properties and new methods of non-equilibrium membrane bound proton fraction research under conditions of proton pump activation, Biochem. Mosc. Suppl. Ser. A: Membr. Cell Biol. **3**, 478 (2009).

[107] C. S. Giometti, T. Khare, N. VerBerkmoes, E. O'Loughlin, and K. Nealson, The Membrane Proteome of Shewanella Oneidensis MR-1, ERSP PI Meeting, Vol. 20 (United States N. p., 2006. Web).

[108] M. Kato, A. V. Pisliakov, and A. Warshel, The barrier for proton transport in aquaporins as a challenge for electrostatic models: The role of protein relaxation in mutational calculations, Proteins Struct. Funct. Bioinforma. **64**, 829 (2006).

[109] G. Acbas, K. A. Niessen, E. H. Snell, and A. G. Markelz, Optical measurements of long-range protein vibrations, Nat. Commun. **5**, 3076 (2014).

[110] J. Brudermann, P. Lohbrandt, U. Buck, and V. Buch, Surface Vibrations of Large Water Clusters by He Atom Scattering, Phys. Rev. Lett. **80**, 2821 (1998).

[111] P. G. Righetti and T. Caravaggio, Isoelectric points and molecular weights of proteins: A table, J. Chromatogr. A **127**, 1 (1976).

[112] A. Van-Quynh, S. Willson, and R. G. Bryant, Protein reorientation and bound water molecules measured by 1H magnetic spin-lattice relaxation, Biophys. J. **84**, 558 (2003).

[113] S. Kiihne and R. G. Bryant, Protein-bound water molecule counting by resolution of 1H spin-lattice relaxation mechanisms, Biophys. J. **78**, 2163 (2000).

[114] V. P. Denisov and B. Halle, Protein hydration dynamics in aqueous solution, Faraday Discuss. **103**, 227 (1996).

[115] A. A. Rashin, M. Iofin, and B. Honig, Internal cavities and buried waters in globular proteins, Biochemistry **25**, 3619 (1986).